Scaling theory reveals weak and changing river flow regulation in a medium-size tropical basin

Diver Eduardo Marín Palacio

Tesis de maestría presentada para optar al título de Magíster en Ingeniería Ambiental

Tutor
Juan Fernando Salazar Villegas, Doctor (PhD) en Recursos Hidráulicos

Universidad de Antioquia
Facultad de Ingeniería
Maestría en Ingeniería Ambiental
Medellín, Antioquia, Colombia
2022

Cita	(Marín, D.E & Salazar J.F, 2022)
Referencia **Estilo APA 7 (2020)**	Marín, D.E & Salazar J.F. (2022). *Scaling theory reveals weak and changing river Flow regulation in a medium-size tropical basin* [Tesis de maestría]. Universidad de Antioquia, Medellín, Colombia.

Maestría en Ingeniería Ambiental, Cohorte Seleccione cohorte posgrado.

Grupo de Investigación Ingeniería y Gestión Ambiental (GIGA).

Seleccione centro de investigación UdeA (A-Z).

Agradecimientos

Le doy gracias a Dios por haberme permitido emprender este camino, por guiarme y darme las herramientas para seguir adelante y dar siempre lo mejor de mí.

A mis padres y hermano, quienes siempre han confiado en mí y han sido mi soporte e inspiración para afrontar cada uno de los retos y desafíos de mi vida.

A Laura Aponte, quien ha sido apoyo e inspiración para creer en mí y soñar en grande.

A mi asesor, el profesor Juan F. Salazar, quién me brindó su confianza, apoyo y conocimiento.

A mi amigo y colega Santiago Valencia por el apoyo y el conocimiento compartido.

A mis colegas y amigos Derly Gómez, Andrés Octavio Pérez Brand, Diana Atehortúa, Elizabeth Ocampo, Santiago Londoño, Isabel Acero y Heli Arregoces por su retroalimentación y acompañamiento en mi proceso de maestría.

A mis amigos Andrés Medina, Pascual Medina, Mateo Londoño, Santiago Gaviria y Juan Pablo Pino, por su amistad, confianza y apoyo incondicional.

A la Universidad de Antioquia por el apoyo otorgado mediante la beca de maestría de la Facultad de Ingeniería.

ABSTRACT

How and why river flow changes due to environmental change are essential questions for hydrological sciences and society. Based on previous studies relating the scaling properties of river flow to a basins' regulation capacity, here we use the scaling theory to investigate changes in a medium-size tropical basin (the Magdalena river basin)'s capacity to regulate extreme flows over 1992-2015. Regulation is defined here as the basin's capacity to either dampen high flows or enhance low flows, which depends on how a basin stores and releases water through time. In contrast to most previous studies, we focus on the scaling properties of events rather than long-term averages. A jump in the scaling exponents reveals that the basin's capacity to regulate low flow has weakened after 2010, which we relate to a decreasing trend in terrestrial water storage that can affect the basin's capacity to enhance low flow through base flow. Scaling exponents above one reveal that the basin has had a weak capacity to regulate its high flow throughout the study period, which we relate to the spatial variability of rainfall and land use/land cover. Despite the focus on the Magdalena river basin, our study provides theoretical and applied foundations for using the scaling laws in understanding temporal changes of river flow regimes and the basins' regulation capacity. This understanding is critical for water management and related decisions in a changing environment.

Keywords: Scaling theory, extreme river flows, non-stationarity, hydrological regulation, Panta Rhei

1. INTRODUCTION

Some of the main problems in hydrological sciences are related to how and why river flow changes due to environmental change and the concomitant impacts on society and ecosystems (Li et al., 2017; Best, 2019). Extreme flows (i.e., high and low flows) are critical due to their relationship with floods and droughts. For instance, in Colombia, La Niña 2010-2011 caused severe floods in extensive areas and related economic losses roughly estimated at US 7.8 billion (Hoyos et al., 2013); whereas El Niño 2015-2016 caused extreme low flows linked to droughts

that compromised water availability for many people (Hoyos et al., 2017) and hydropower generation (Weng et al., 2020).

Non-stationarity of hydrological phenomena is a critical problem for hydrological sciences. Montanari et al. (2013) described this as Panta Rhei ("everything flows") to highlight the challenge of understanding hydrologic dynamics in a changing environment. In general, the river flow regime in a basin results from a complex aggregation process at different scales that depends on multiple factors such as climate, land use/land cover (LULC), and geomorphology (Zhang et al., 2018; Salazar et al., 2018). The scaling theory has been proposed as a theoretical and applied framework to deal with these processes and their inherent complexity and heterogeneity in river basins (Gupta et al., 2007). A central idea of this theory is that some properties exhibit scale-invariance, meaning, for instance, that they do not vary with increasing spatial scale in a river basin. The scale-invariance is a consequence of the system´s internal dynamics and self-organization, and it implies a power-law correlation between the system (e.g., a river basin) response (e.g., streamflow) and a scale parameter (e.g., the catchment area), that is (Salazar et al., 2018)

$$E[Q_i^k] = \alpha_i A^{\beta_i}, \quad (1)$$

where $E[Q_i^k]$ is the k-th order statistical moment of the probability distribution function of low (Q_L, i=L) or high (Q_F, i=F) flow, A is the catchment area (scale parameter), and α_i and β_i are the scaling parameter and coefficient (or prefactor), respectively. Non-stationarity means that the scaling exponent and coefficient vary with time (Rodríguez et al., 2018).

Although some exceptions focused on mean or low flows (Vogel & Sankarasubramanian, 2000; Modarres, 2010; Rodríguez et al., 2018), previous studies have focused mainly on floods (Gupta et al., 1994; Gupta & Dawdy, 1995; Gupta, 2004; Gupta et al., 2015; Ayalew, 2018; Perez, 2018), using two main approaches: modeling of idealized basins (e.g., Gupta, 1996; Menabde et al., 2001; Mantilla et al., 2006; Ayalew et al., 2014) and observation-based analysis of actual basins (e.g., Gupta & Dawdy, 1995; Ogden et al., 2003; Ayalew et al., 2018; Perez et al., 2018). Moreover, most studies have analyzed the scaling properties based on flows' annual statistics (e.g., Gupta & Dawdy, 1995; Eaton et al., 2002; Gupta et al., 2010; Rodríguez et al., 2018). An alternative is to study the scaling properties for specific high or low flows events rather than annual statistics (e.g., Gupta, 2004; Ayalew et al., 2014; Furey et al., 2016). In both cases, the scaling properties are computed from high or low flow data at different locations

(gauges) in the basin's drainage network. When using annual statistics, there is no synchronicity between high or low flows in different gauges, i.e., these extreme flows do not correspond to the same event. In contrast, the event approach uses synchronous flows to obtain the scaling properties, thereby focusing on how the flow changes with increasing spatial scale leading to an extreme event in the basin outlet.

A fundamental question for the scaling theory in hydrology is how the scaling properties (mainly the scaling exponent) relate to physical phenomena (Gupta et al., 1994; 2007). Previous studies have related flood's scaling properties to differences between snowmelt- or rainfall- generated floods (Gupta and Dawdy, 1995; Eaton et al., 2002), the fractal properties of the drainage network and rainfall (Gupta, 1996), the excess intensity and rainfall duration (Gupta et al., 1998; Menabde et al., 2001), actual network structures and flow dynamics (Mantilla, 2006), and the spatio-temporal variability of rainfall (Mandapaka et al., 2009). Other studies focused on the regional flood frequency analysis (RFFA) and the use of scaling laws to describe river floods over homogeneous regions (Eaton et al., 2002; Ishak et al., 2011; Perez, 2019), as well as on the application of different regression models to investigate different variables' role in generating flood peaks (Farmer et al., 2015; Perez, 2019; Formetta et al., 2021).

Studying the Amazon river basin, Salazar et al. (2018) related the scaling properties of a river basin to its regulation capacity, defined as the basin's capacity to dampen high flows and amplify low flows under the influence of, e.g., high or low rainfall, respectively. These dampening and amplification processes depend on how basins store and release water through time, which involves complex and dynamic phenomena occurring within basins and sensitive to environmental change. Building on this study, Rodríguez et al. (2018) showed that the scaling exponents of large Amazon sub-basins and the Magdalena river basin have changed over time and interpreted these changes as evidence of non-stationarity in the basins' regulation capacity. Both studies used annual statistics from high and low flows measured asynchronously across the gauging network.

Here we study the scaling properties in the Magdalena River Basin (MRB henceforth) for annual events of high and low flows, i.e., using synchronous flow measures (further details in Section 2). As we will show below, this leads to substantially different results from the previous study by Rodríguez et al. (2018) and provides new insights on the physical processes behind

the scaling properties and the basin's hydrological dynamics. The MRB is the most important basin for water and energy security in Colombia, including being the place of many economic activities and home for most of the country's population (Angarita et al., 2018; Restrepo et al., 2015). Our aims are, first, to characterize the temporal evolution of scaling properties in the MRB for high and low flow events, then to investigate how the MRB's regulation capacity has behaved over time based on the scaling exponents, and, finally, to explore the physical processes behind the resulting patterns.

2. DATA AND METHODS

2.1 Study area

The MRB (Figure 1) located in northwestern South America, flows across Colombia with a length of about 1,105 km and a catchment area around 160,914 km². The river originates in the Andes mountains at around 3,700 m.a.s.l and flows towards its mouth in the Western Caribbean Sea (Restrepo & Kjerfve, 2000). The average annual precipitation in the MRB is ~1,989 mm, with a bi-modal seasonal cycle mainly related to the seasonal migration of the Inter-tropical Convergence Zone (ITCZ; Urrea et al., 2019), and pronounced interannual variability primarily modulated by El Niño Southern Oscillation (ENSO, Poveda, et al., 2002). The average annual discharge at the basin outlet is ~ 4,154 $m^3 s^{-1}$, ranging from 1,252 $m^3 s^{-1}$ to 9,217 $m^3 s^{-1}$ (1992-2015). Our analysis does not set the basin outlet in the Caribbean Sea but in the El Banco gauge (Figure 1) due to the number and distribution of gauging stations with streamflow data available for the study period and covering multiple spatial scales, as required for the scaling analysis.

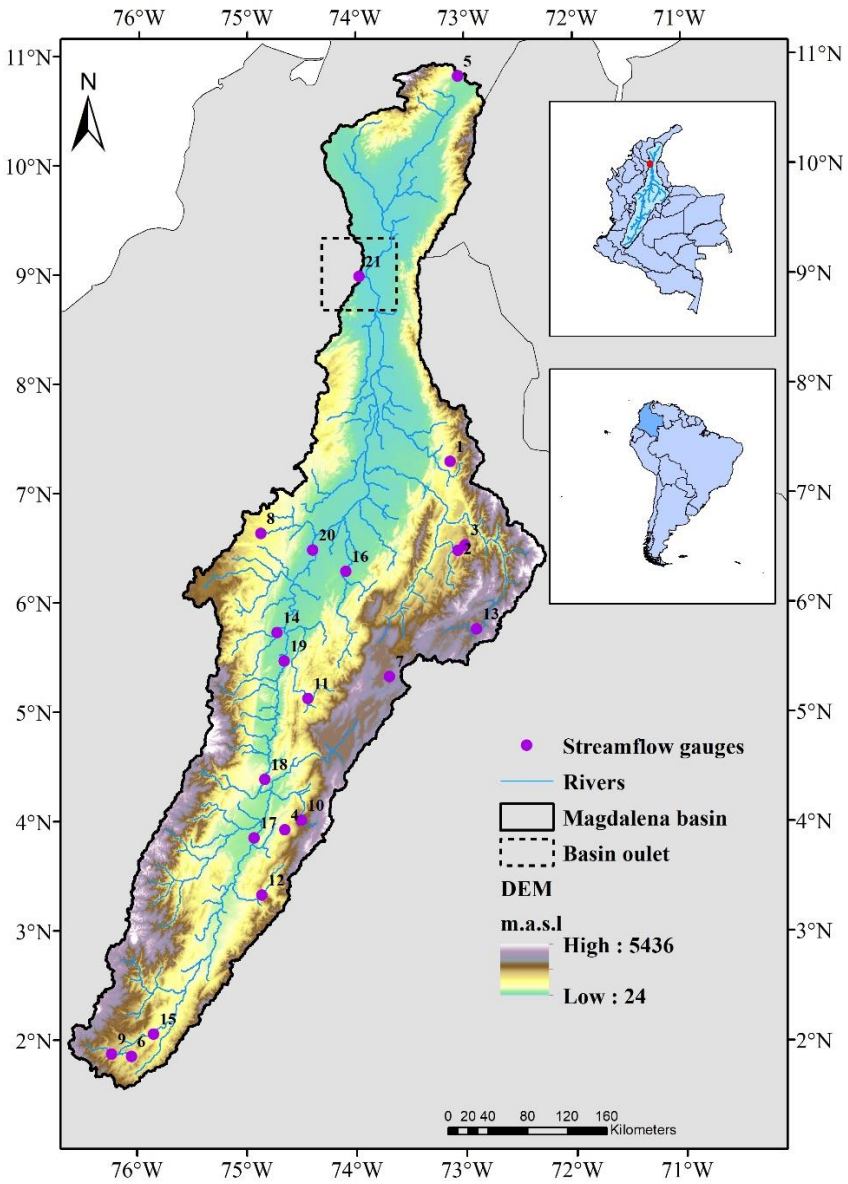

Figure 1. The Magdalena River Basin (MRB) in northwestern South America. Topography (shading) and streamflow gauging stations (points). Gauge numbers grow with increasing catchment area from 125 km^2 to 160,914 km^2. Details in Table 1.

2.1 Data

For the scaling analysis, we used daily streamflow data for 1992-2015 measured at the 21 gauges shown in Figure 1 and described in Table 1, provided by the Institute of Hydrology, Meteorology and Environmental Studies of Colombia (IDEAM, http://www.ideam.gov.co/). These gauges were identified after filtering the original database (475 gauges, 1950-2019) with a threshold of 12.5% of missing data per year (i.e., half of a 3-months season) for the study

period (1992-2015). This analysis of data availability was the basis for setting the basin outlet at the El Banco gauge (gauge 21 in Figure 1) rather than near the Caribbean Sea.

Table 1. Gauging stations for daily streamflow.

IDEAM Code	Area (km^2)	Latitude	Longitude	Elevation (m.a.s.l)	ID (Figure 1)
25027020	160,914	8.99	-73.96	29	21
23097030	74,387	6.48	-74.4	111	20
23037010	56,500	5.46	-74.66	186	19
21237010	48,100	4.38	-74.83	277	18
21137010	25,485	3.84	-74.93	306	17
23127060	4,901	6.29	-74.09	154	16
21027010	3,561	2.05	-75.85	839	15
23057140	2,335	5.73	-74.72	176	14
24037290	2,092	5.75	-72.9	2,490	13
21147030	1,668	3.32	-74.86	730	12
23067060	1,116	5.12	-74.44	620	11
21197010	958	4.01	-74.5	1,860	10
21017020	319	1.87	-76.23	1,233	9
23107030	307	6.63	-74.87	970	8
24017610	289	5.32	-73.69	2,590	7
21017050	268	1.84	-76.05	1,250	6

28017080	206	10.81	-73.05	275	5
21167060	202	3.92	-74.65	744	4
24027040	184	6.52	-73	1,700	3
24027060	165	6.47	-73.07	1,223	2
23197130	125	7.29	-73.14	770	1

We used Precipitation (P), Terrestrial Water Storage (TWS), and Land Use Land Cover (LULC) data to complement the scaling analysis. P is from the Climate Hazards Center InfraRed Precipitation with Station data (CHIRPS version 2), which is a gridded dataset that provides blended gauge-satellite precipitation estimates that cover most global land regions with a high resolution (0.05°) and a long period of records (1981-present; Funk et al., 2015). Particularly, this dataset has a suitable performance for the MRB (Supplementary figure S4). Monthly TWS (April 2002 to December 2015) is from the Mascons (mass concentrations functions) product provided by the Jet Propulsion Laboratory after processing GRACE data, which is a gridded product with a spatial resolution of 0.5° that use mass concentrations functions (i.e., Mascons) to parameterize the gravity field (Watkins et al., 2015; Save et al., 2016). Bolaños et al. (2021) identified this product as the best GRACE-based product representing TWS in the MRB. LULC data is from the Land Cover CCI global dataset (ESA, 2017; e.g., Li et al., 2016; Nowosad et al., 2019) reclassified in the categories defined by the IPCC: forest, croplands, grasslands, shrublands, sparse vegetation, wetlands, urban, bare soils, water, and ice and snow (ESA, 2017). All the information used is summarized in Table 2.

Table 2. Summary of the information used in this study

Sources	**Variable**	**Spatial Resolution**	**Period**	**References**
IDEAM	Streamflow, Q	-	1992-2015	-

CHIRPS v2	Precipitation, P	0.05° (~5.5 km)	1992-2015	Funk et al., 2015
Land Cover CCI	Cover	0.3 km	1992-2015	ESA, 2017
JPL mascons	Terrestrial Water Storage Anomalies, TWS	0.5° (~55.5 km)	Apr 2002-Dec 2015	Watkins et al.,2016; Bolaños et al., 2021
SRTM	Elevation	0.25 km	-	Jarvis et al., 2008

IDEAM: Institute of Hydrology, Meteorology and Environmental Studies of Colombia; CHIRPS: Climate Hazards Group InfraRed Precipitation with Station; ESA: European Space Agency; GRACE: Gravity Recovery and Climate Experiment; SRTM: Shuttle Radar Topographic Mission.

2.2. High and low flow events

Annual high and low flows registered in different points of the drainage network do not correspond to the same event, i.e., they do not occur synchronously in all gauges. When using annual extreme flows or long-term averages to obtain the scaling properties (e.g., Farmer et al., 2015; Formetta et al., 2021; Gupta et al., 2010; Ishak et al., 2011; Rodríguez et al., 2018; Yue et al., 2004), these extremes correspond, generally, to different events at different times (Figure 2a). Here we do not use this approach but obtain the scaling properties for annual events. These events correspond to the annual maximum or minimum flow at the basin outlet, along with the corresponding flows registered simultaneously in all other gauges (Figure 2b). Hence, these other gauges' flows are not necessarily an extreme flow but the flows contributing to the extreme flow at the basin outlet. The resulting scaling properties describe the complex accumulation process leading to extreme flows in the basin outlet and its variability in terms of catchment physical processes. Previous studies used a similar approach, analyzing the scaling properties of peak discharges resulting from individual rainfall-runoff events in nested watersheds and their relationship with the physical characteristics of the catchment and rainfall (e.g., Ayalew et al., 2014; Ayalew et al., 2015; Furey et al., 2016; Perez et al., 2019).

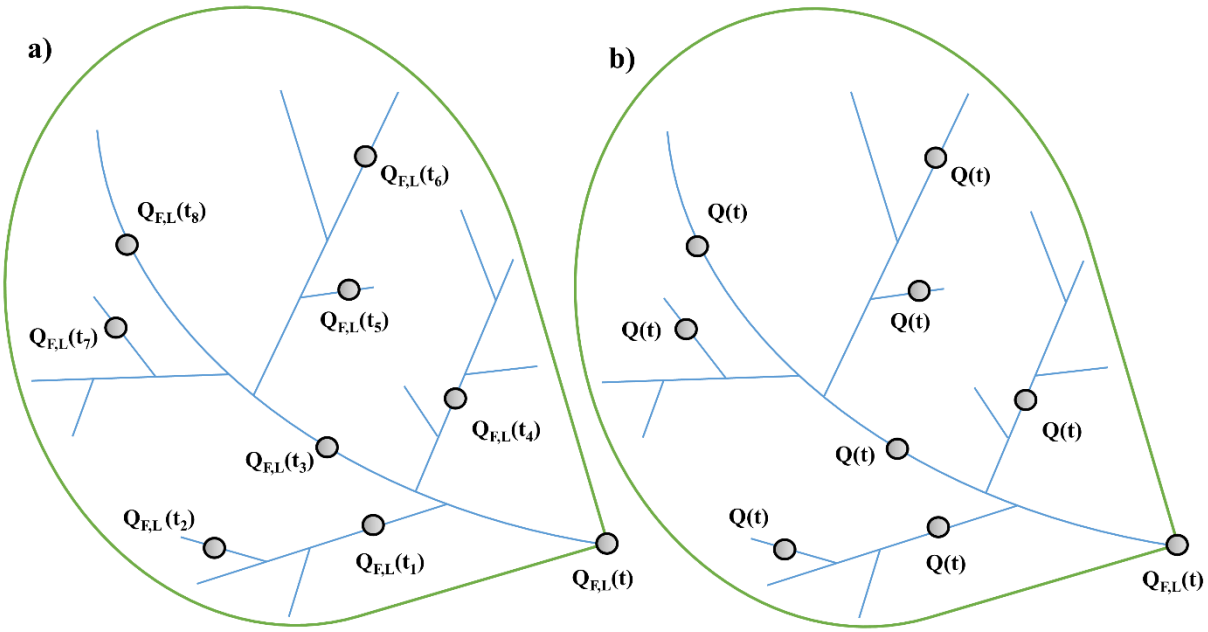

Figure 2. Schematic representation of the (a) annual statistics and (b) event approaches. While flows are not synchronous in (a), they correspond to the same time (t) in (b). $Q_{F,L}$represents high (*F*) or low (*L*) flow at the basin's outlet.

2.3 Estimating scaling laws

Power laws were fitted for extreme river flows to evaluate potential changes in scaling parameters with time. All fitted laws followed the general power law (Eq.(1)), which log-transformed with $k = 1$, is equivalent to:

$$ln(E * [Q_i]) = ln(\alpha_i) + \beta_i ln(A) \quad (2)$$

where $E * [Q_i]$ is a streamflow event for low (i=L) or high (i=F) flows, and other factors are the same as in Eq.(1). We use a star (*) here to highlight that Equation (1) with $k = 1$ do not refer strictly to events but to the mean value over a given time, generally the long-term mean. However, since we are interested in how the scaling properties change with time, we used Eq.(2) to obtain the scaling exponent for different time frames. Hence, we estimated the scaling exponent for each annual event of high and low flows, and also using n-year moving average events with n=2,3,4,5 years (details in Supplementary Table S3). Average events result from averaging flows at each gauge for each time frame (n years), which describe the average flow

accumulation patterns during high or low flows over the n years. This procedure leads to time series of scaling exponents that were used to investigate the said temporal changes.

The scaling coefficient (α_i) and exponent (β_i) were obtained through linear regressions fitted using the standard least-squares method. The statistical significance of these regressions was evaluated with the coefficient of determination (R^2) and p-values. In all cases p-values indicated a significance level of at least 0.001 (details in Supplementary Table S2).

To investigate temporal changes of the time series in MRB (including the scaling exponents and other variables; Table 2), we tested for significant trends and changes in mean values using the non-parametric Trend Free Prewhitening test (TFPW; Tananaev et al., 2016; Mekonnen et al., 2018) and the Mann-Whitney Wilcoxon test, respectively. Both at a significance level of $\alpha = 0.05$.

2.4 Regulation of high and low flows

A river basin can be classified as regulated or unregulated depending on its river flow regime (Salazar et al., 2018). A fundamental feature of this regime is how flows grow with the spatial scale, which is described by the scaling exponents (Figure 3). Regulation is defined here as the basin's capacity to dampen high flows and amplify low flows under the influence of, e.g., high or low rainfall, respectively. Amplification occurs when the runoff contribution to high or low flows per unit area increases downstream, i.e., with increasing spatial scale. This pattern results in a scaling exponent greater than one (β>1). Conversely, dampening occurs when this runoff contribution decreases downstream, leading to a scaling exponent lower than one (β<1). Both amplification and dampening can occur under the most common pattern of increasing streamflow with increasing spatial scale because these processes do not depend on whether Q increases with A (i.e., whether dQ/dA is positive) but on the concavity of the Q vs. A curve (i.e., the sign of the second derivative d^2Q/dA^2; Figure 3). Hence, β=1 is a critical value around which the curvature of the power-law (Eq.1) changes. From this perspective, a higher regulation in a river basin implies both reducing floods through dampening effects produced by water retention within the basin and increasing low flows through amplification effects resulting from the release of water stored within the basin (Salazar et al., 2018).

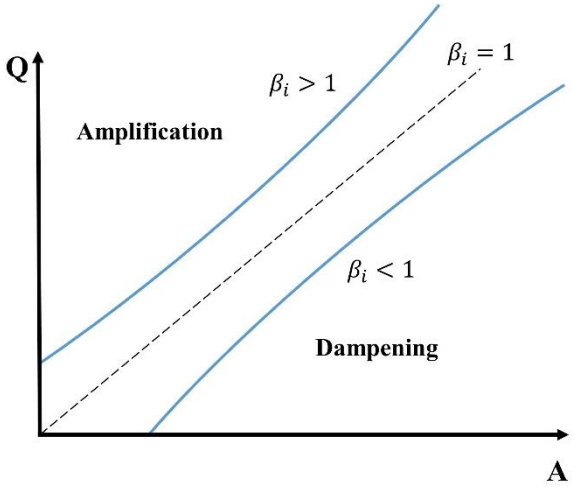

Figure 3. Schematic representation of the amplification and dampening process in a basin. The Y-axis represents the streamflow and the X-axis the basin's area. The blue lines represent how the streamflow grows with the scale.

2.5 Precipitation and land use/land cover change analysis

To explore mechanisms behind the scaling properties, we analyzed precipitation during and before the day of each high flow event. Using data from CHIRPSv2, we obtained maps for daily mean precipitation during each event and 30-days accumulated precipitation before each event for the MRB. The rationale is that high flows are generated primarily by precipitation falling during a particular day and depend on antecedent moisture, which is uncertain but related to precipitation before the event and critical for flood generation (Brunner et al., 2021; Brunner et al., 2020). Furthermore, we obtained a time series of the amplitude of monthly precipitation by regions (the Northern and Southern parts of the basin) as the difference between the monthly highest and lowest precipitation value per year.

Additionally, using annual land cover maps from ESA, we considered spatio-temporal changes of LULC in the basin over the study period. Categories were reclassified following the classification proposed by the Intergovernmental Panel on Climate Change (IPCC; ESA, 2017). The modal value of each pixel was used to describe the predominant LULC over time. Using the Kappa index (Badia et al., 2019; Cohen, 1960) to compare annual LULC maps, we investigated temporal changes in LULC.

3.RESULTS AND DISCUSSION

3.1 Synchronicity of low and high flows

Low flows do not co-occur in all gauges, i.e., there is no synchronization among low flows in all sub-basins (Figure 4a). This supports our event-based approach in which the scaling exponent and prefactor describe the accumulation process that produces low flow in the basin outlet. In most cases, low flow occurs during or after the first dry season of the year (DJF), which, on average, is the driest season in the MRB (Figure 5). However, there are exceptions, such as gauges 11 and 14, where low flow concentrates in August after the second dry season of the year.

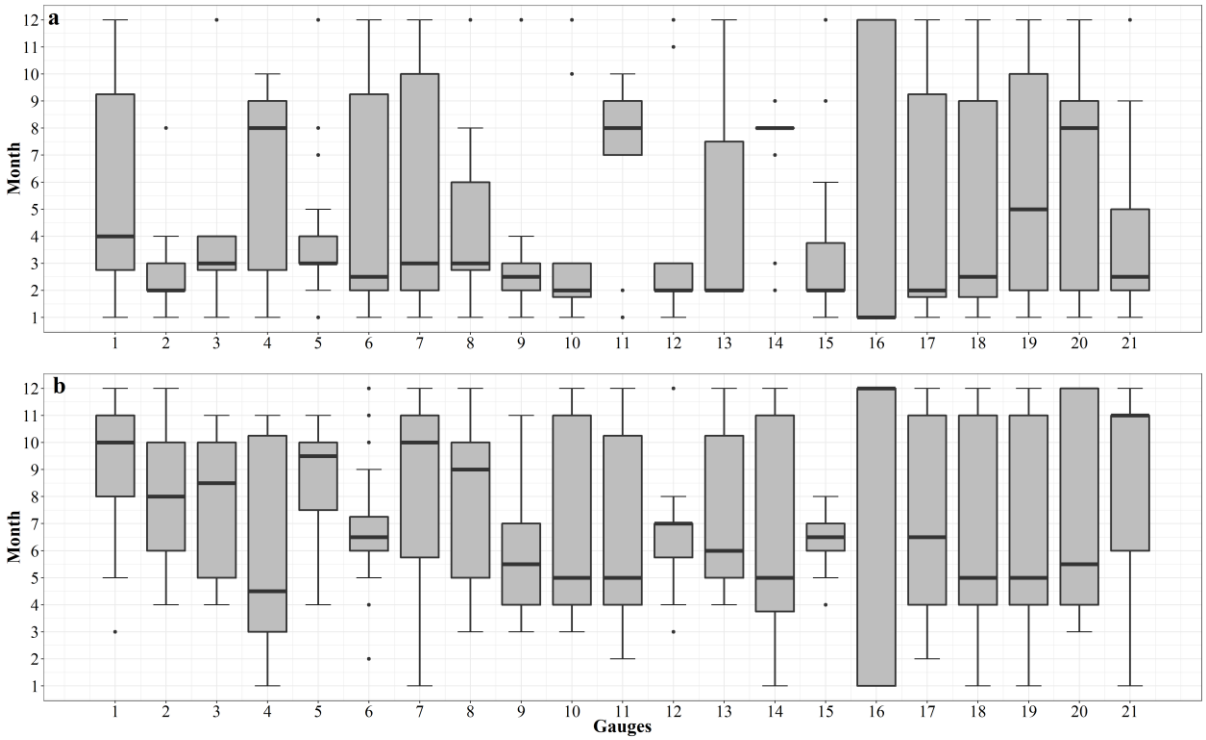

Figure 4. Lack of synchronization of annual low (a) and high (b) flows among MRB's sub-basins. The Y-axis shows the month of occurrence of annual low or high flows in different sub-basins. Box-plots show variability over 1992-2015 Numbers in the X-axis identify sub-basins, as shown in Figure 1.

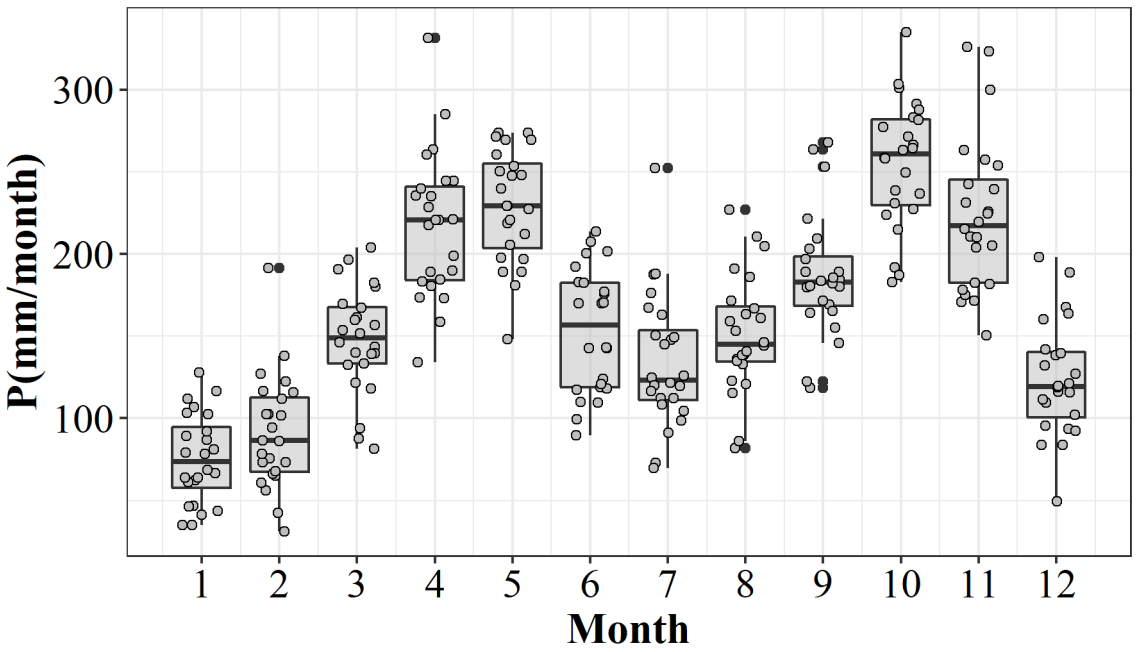

Figure 5. Annual cycle of precipitation (P) in the MRB. Values from CHIRPS are averaged over the basin. Box-plots describe variability among years in the time series.

Likewise, high flows do not occur synchronously among all sub-basins (Figure 4b). Although they occur mainly during the second wet season of the year (SON; Figure 5), there are gauges where high flow had happened in any other month (e.g., gauge 16). The high flow concentration around SON may be a consequence of the difference between the first (DJF) and second (JJA) dry seasons. Since the latter is less dry (Figure 5), soils may approach saturation more rapidly during SON than during MAM (the first wet season), enhancing high flows and floods in SON.

3.2 Scaling exponent for low flows

Figure 6a shows that the scaling exponent for low flow (β_L) has been most of the time greater than 1, regardless of using yearly values of moving averages to estimate them. Values above 1 indicate that the basin behaves as regulated, meaning that it amplifies low flow as the spatial scale increases (Salazar et al., 2018). However, a statistically significant change in their mean reveals that β_L values are getting closer to 1 over the last few years, which indicates a weakening of the basin's regulation capacity for low flow (Rodríguez et al., 2018).

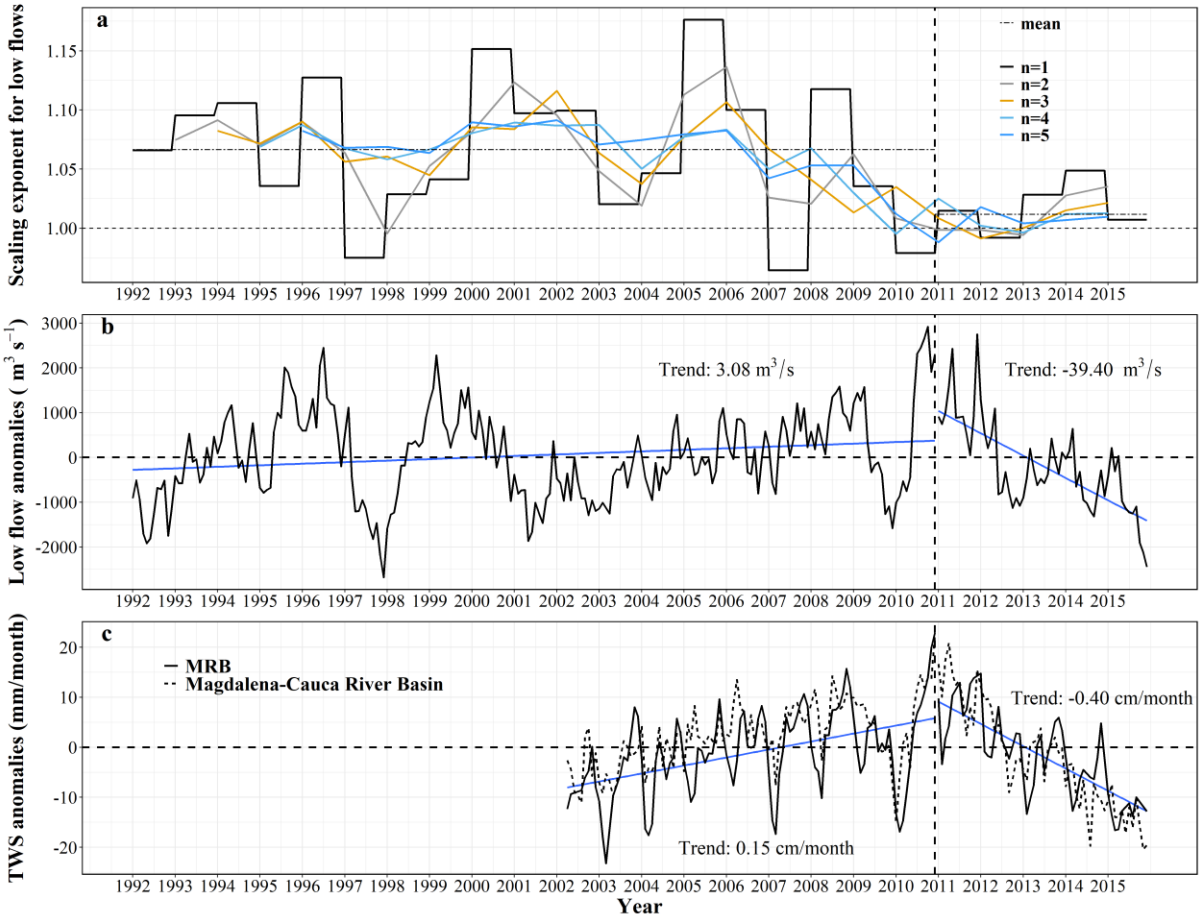

Figure 6. Time series of (a) scaling exponent for low flow based on yearly values and moving averages, where the two dotted black line represents the mean before December 2010 and afterwards, and the dashed thin line represents the critical value of the scaling exponent. (b) Monthly low flow anomalies, where the blue lines show significant trends, which are positive before December 2010 and negative afterwards. (c) monthly TWS in the MRB represented by a solid black line and TWS in the Magdalena-Cauca River Basin represented by a dashed black line. The solid blue lines represent trends before and after December 2010. The jump in the mean in panel (a) and trends in panels (b and c) are statistically significant ($p < 0.05$).

The behavior of the scaling exponent for low flow over time differs from Rodríguez et al.'s (2018) findings. This previous study found a shift from an unregulated to a regulated state, linked to an increasing trend in the basin's capacity to regulate low flows. This difference between Rodriguez et al.'s (2018) finding and ours results from using the event approach in the present study. Whereas Rodriguez et al. (2018) used the standard practice of considering annual statistics from each gauge despite being asynchronous, we examined the scaling exponents for low flow events, which requires synchronicity among gauges. Nevertheless, both

studies indicate that the low flow scaling exponent is close to 1 (i.e., the critical value) in recent years.

The change in the scaling exponent β_L in 2010 coincides with statistically significant changes in the time series of low flow anomalies (Fig. 6b) and TWS (Figure 6c) obtained from GRACE. In 2010, basin-average low flow anomalies changed from an increasing (3.08 $m^3 s^{-1}$) to a decreasing (-39.40 $m^3 s^{-1}$) trend. Notably, these changes coincide with a change in TWS identified by Bolaños et al. (2020) for the whole Magdalena river basin (including the Cauca river, greater than our study MRB), indicating that both surface and groundwater storage have been reducing during 2010-2017, perhaps as a consequence of transitioning between strong ENSO phases: La Niña in 2010-2011 and El Niño in 2015-2016. The same pattern occurs in the MRB, as shown by the solid black line in Figure 6c.

Changes in low flow anomalies and TWS are likely related to the identified weakening of low flow regulation. Low flow occurs due to prolonged periods with low precipitation in which streamflow depends strongly on base flow. In turn, this base flow depends primarily on water storage. TWS reduction can weaken base flow and, therefore, the basin's capacity to amplify low flows during dry seasons.

3.3. Scaling exponent for high flows

There are neither significant trends nor changes in its mean for β_F, and high flow anomalies and precipitation anomalies in the basin do not exhibit significant trends or changes either. Nevertheless, the scaling exponent for high flow (β_F) indicates that the MRB behaves mostly as unregulated. This follows from values of β_F being greater than one most of the time (Figure 7a) and the physical interpretation of scaling exponents proposed by Salazar et al. (2018) and Rodríguez et al. (2018). In an unregulated basin, β_F>1 indicates that the basin does not dampen but amplifies high flow. Conversely, a regulated basin dampens high flow, which manifests in a scaling exponent lower than one.

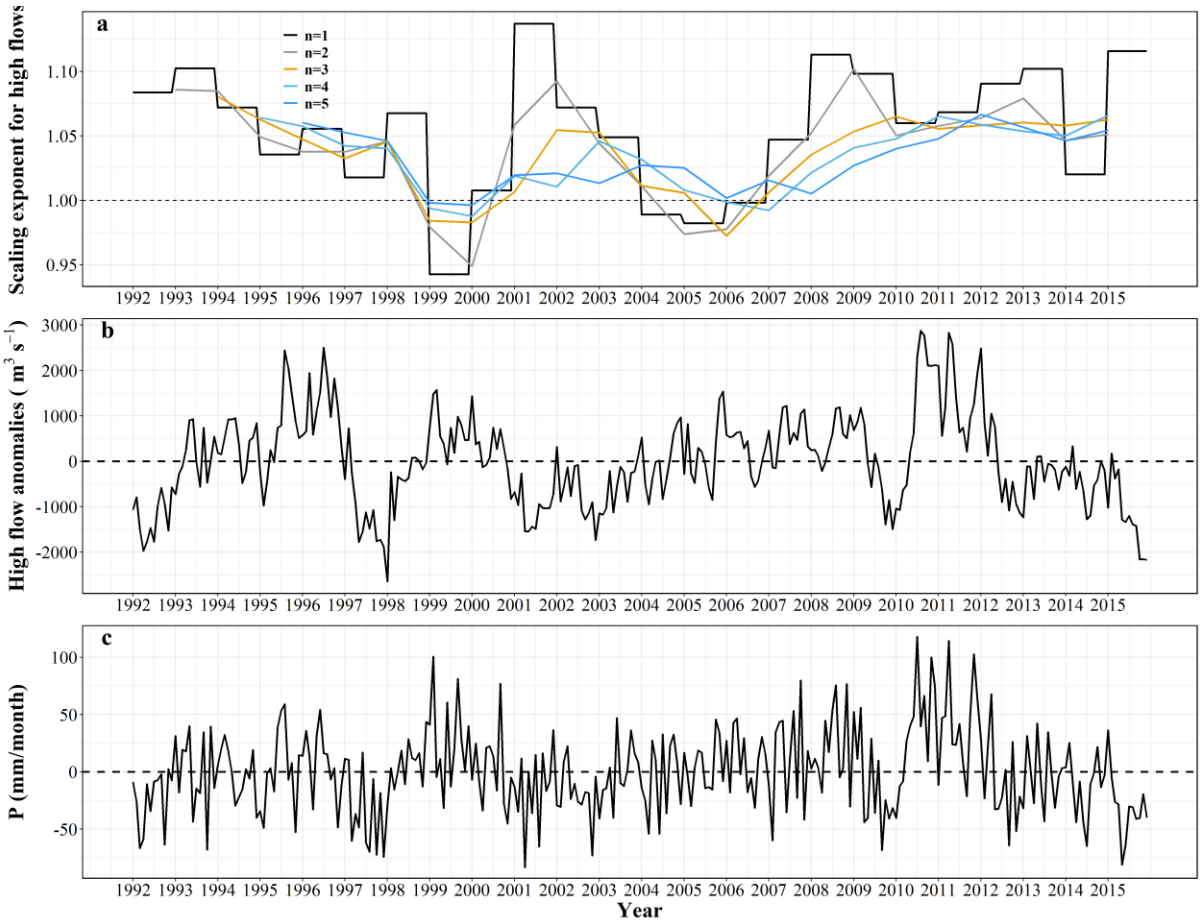

Figure 7. Time series of (a) scaling exponent for high flows based on yearly values and moving averages. The dashed thin line represents the critical value for the scaling exponent. b) Monthly high flows anomalies and, c) Monthly precipitation anomalies (P) for MRB.

Non-regulation of high flows in the MRB is an unexpected result because this basin has a well-developed system of dams and reservoirs, including more than 33 dams in operation along the Magdalena river (Angarita et al., 2018). However, these dams and reservoirs are not operated for flood control but mainly for hydropower generation, i.e., based primarily on economic criteria related to the Colombian energy stock market (Barrientos & Villada, 2014). Besides not being conceived and operated for flood control, these dams and reservoirs are related to widespread changes in the basin (e.g., the effects of damming the Amazon; Latrubesse et al., 2017) that can weaken its natural regulation capacity (Salazar et al., 2018).

High flow scaling exponents greater than 1 is an unexpected result also because it contradicts the theoretical limit suggested by Gupta (2004), as well as the most common results from previous studies: β_F<1 (Lima et al., 2017; Perez et al., 2018; Perez et al., 2019). Nevertheless, Ayalew et al. (2015) noted that this theoretical limit depends on the underlying assumption that

precipitation intensity causing floods is homogeneous throughout the basin. This assumption does not hold for the MRB basin; instead, there is high precipitation variability during the specific day of flood occurrence (Figure 8a and Supplementary Figure S2) and the previous month (30 days; Figure 8b and Supplementary Figure S3). This latter is important for soil saturation, a critical process in flood production. Furthermore, our event approach does not coincide with most previous studies, including Rodríguez et al. (2018)'s that found β_F<1 in the same basin, suggesting that synchronization makes significant differences in estimating scaling properties.

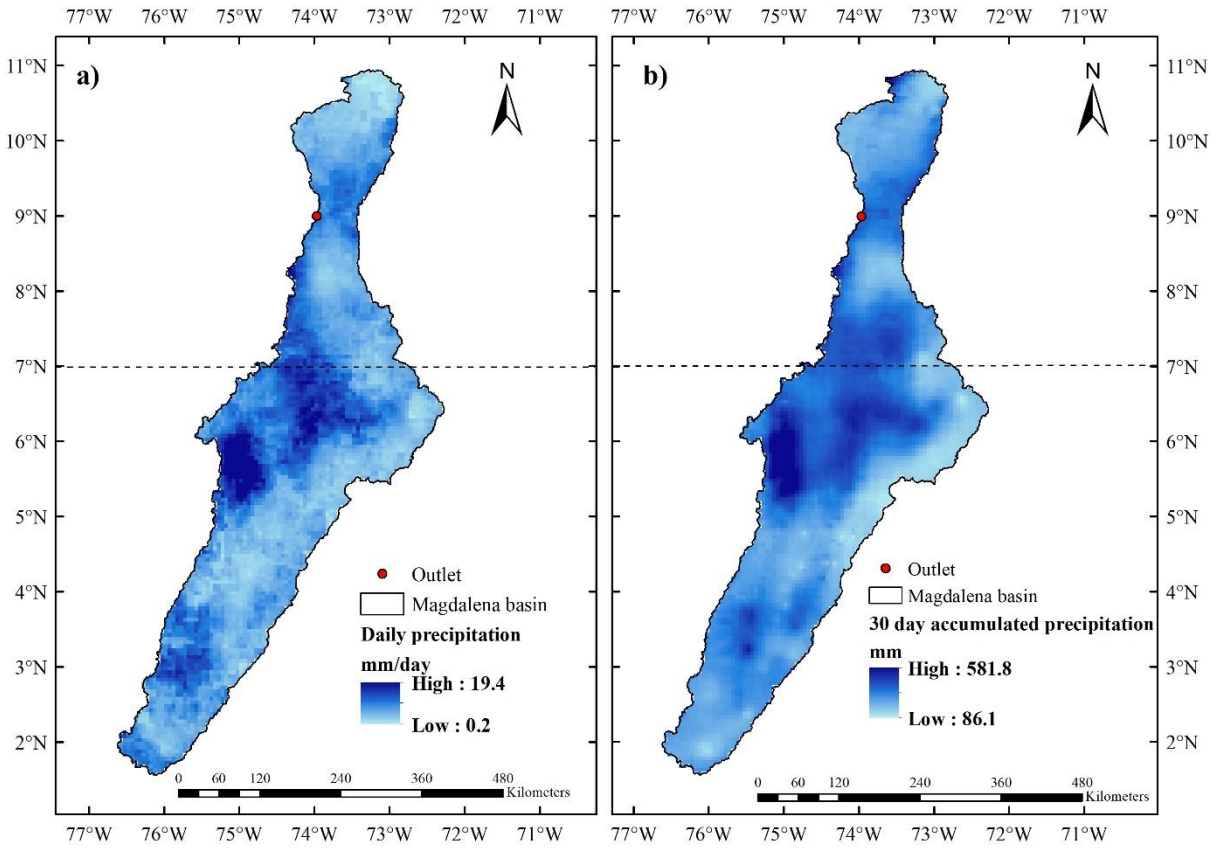

Figure 8. a) Daily mean precipitation during high flow events. b) 30-days mean accumulated precipitation before high flow events. Dashed line divides the basin into Northern (7°N-11°N) and Southern (1.5°N-7°N) parts.

The average daily precipitation during high flow events (Figure 8a) and 30-day antecedent precipitation (Figure 8b) are not distributed homogeneously over the basin. Instead, higher precipitation values concentrate mostly around the center part of the basin, not so far from its outlet. This precipitation pattern partly explains why high flows amplify downstream. The contribution to high flow (per unit area) of any area fraction of the basin can grow with

increasing area simply because the basin receives more precipitation in its center than in its upper (southern) part.

Figure 9 shows the precipitation annual cycle and its amplitude in the Northern (7°N-11°N) and Southern (1.5°N-7°N) parts of the basin. On average, monthly precipitation reaches more extreme values in the Northern than in the Southern part (Figure 9a), including the highest precipitation in October during the second wet season and the lowest precipitation in January during the first dry season. Over time, the precipitation's annual cycle amplitude is greater in the North than in the South (Figure 9b). The amplification of high flows revealed by the scaling exponent (β_F>1) implies that, per unit area, the Northern part of the basin contributes more to high flows at the basin outlet than the Southern part. This amplification seems consistent with the described features of the precipitation regime with marked North-South heterogeneity and a more extreme wet season in the North, which is the lower part of the basin near its outlet.

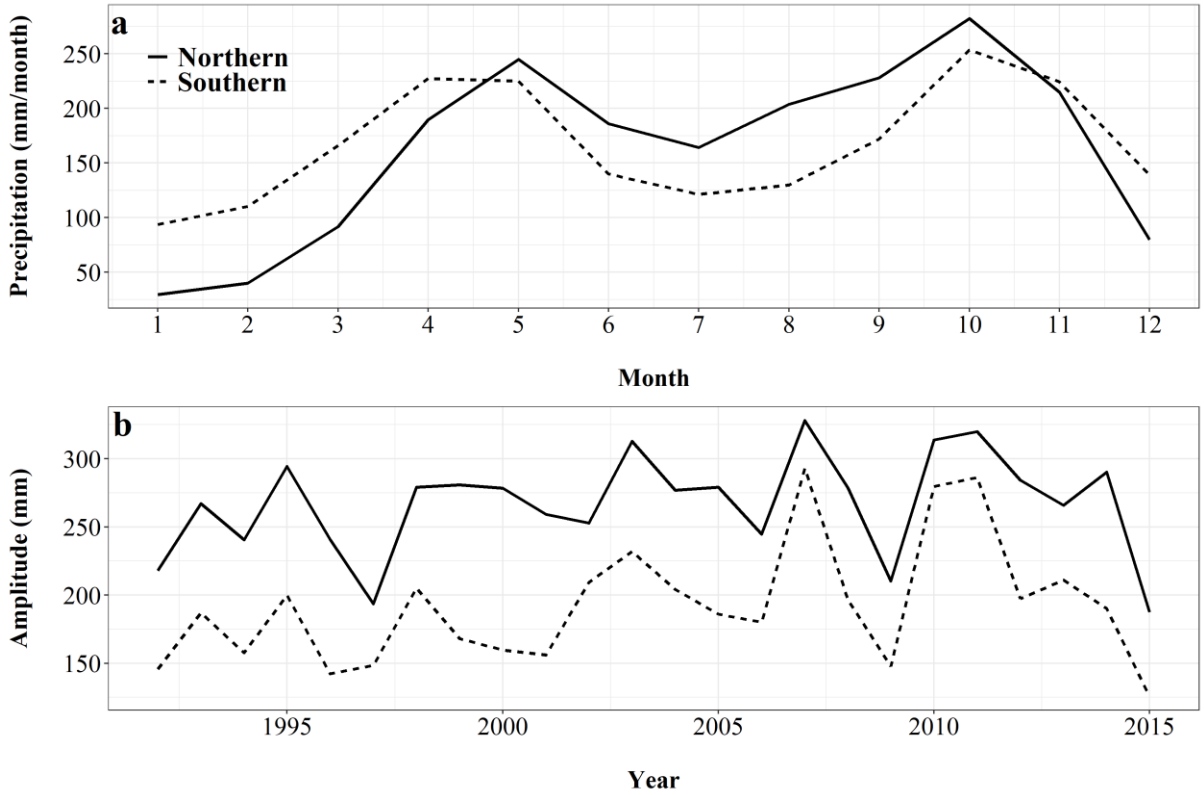

Figure 9. a) Average (1992-2015) annual precipitation cycle for the Northern and Southern parts (indicated by the dashed line in Fig. 6) of the MRB. b) Yearly amplitude of the precipitation annual cycle: difference between the highest and lowest precipitation value of the annual cycle per year.

Figure 10 shows the most common LULC class (i.e., the modal) in the basin based on annual maps from 1992 to 2015 (Supplementary Figure S1). As for precipitation, LULC shows a pronounced Northern-Southern heterogeneity. Whereas agricultural land predominates in the North, forest and shrubland predominate in the South. Since LULC is critical for streamflow production in a basin (Dosdogru et al., 2020; Ellison et al., 2017; Peña-Arancibia et al., 2019; Zhang et al., 2018), this LULC heterogeneity affects how the Northern and Southern parts of the basin contribute to high flow in the basin outlet. Previous studies in the region indicate that, compared to forest and shrubland, agricultural land is less effective in maintaining higher levels of soil moisture and decreasing potential overland flow, contributing to hydrological regulation (García-leoz et al., 2018). Furthermore, tropical forests may be critical for increasing basins' capacity to regulate river flow, including floods dampening (Bonnesoeur et al., 2019; Salazar et al., 2018). Hence, high flow amplification (β_F>1) in the Magdalena basin seems generally consistent also with its LULC heterogeneity.

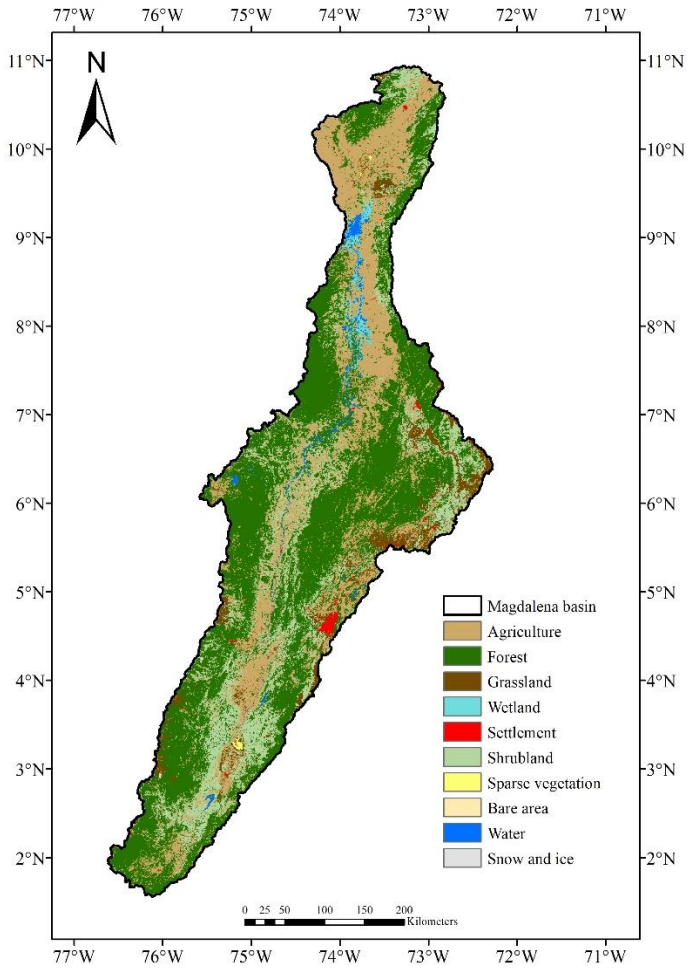

Figure 10. Land cover and land use in MRB for 1992-2015. Each pixel on the map is represented by the modal value (i.e., the most frequent value) for the study period.

4.CONCLUSIONS

We used the scaling theory for studying changes in the MRB's capacity to regulate its extreme river flows. In contrast to most previous studies, we focused on the scaling properties of "events" here characterized by sets of observed river flows that co-occurred, i.e., assuring synchronization between flow records at a daily scale (the available resolution). Hence, the analyzed scaling properties relate to how flow aggregates across the basin's river network when annual high or low flow occurs at the basin's outlet.

Scaling exponent values above one indicate that the MRB has behaved as regulated for low flow during the last decades (1992-2015), i.e., the basin enhances low flow with increasing spatial scale. However, this regulation capacity has weakened recently, as indicated by a considerable reduction of the scaling exponent after 2010. Although the behavior remains regulated, the scaling exponent getting closer to one indicates that the basin has approached a state where it would not amplify (regulate) but dampen low flow. This regulation weakening coincides with a decreasing trend in terrestrial water storage revealed by GRACE data, which we relate to a weakening in the basin's capacity to enhance low flow through base flow.

Scaling exponent values above one indicate that the MRB has behaved as unregulated for high flow during the last decades, i.e., the basin does not dampen high flow with increasing spatial scale. This result is unexpected because most previous studies have reported high flow's scaling exponent values lower than one. However, we relate this MRB's feature with its size (most previous studies focused on smaller basins) and pronounced spatial variability of rainfall and LULC. In contrast to low flow, we did not find significant changes in the time series of the scaling exponent for high flow. In particular, we did not find a relationship between temporal changes in LULC and the scaling exponents

Studying the whole Magdalena-Cauca river basin, which in contrast to the present study, includes the Cauca river, Rodriguez et al. (2018) did not find either low flow regulation weakening or high flow unregulation. These differences arise from using the event approach in the present study, which, due to data analysis and availability, implied focusing on a sub-basin (the MRB) that excludes the Cauca river. Furthermore, these differences suggest that the event approach may introduce significant differences in estimating the scaling properties that future studies should further consider.

This study provides theoretical and applied foundations for using the scaling laws to understand temporal changes of river flow regimes, particularly regarding changes in the basins' regulation capacity. This understanding is critical for water management decisions and water security assessments in a changing environment.

DATA ACCESSIBILITY

The original data used in this work are all publicly available from their sources IDEAM: http://www.ideam.gov.co/, CHIRPSv2:https://data.chc.ucsb.edu/products/CHIRPS-2.0/, ESA: http://maps.elie.ucl.ac.be/CCI/viewer/download.php,TWS:https://podaac.jpl.nasa.gov/dataset/TELLUS_GRACGRFO_MASCON_CRI_GRID_RL06_V2,SRTM:https://srtm.csi.cgiar.org/srtmdata/ .

ACKNOWLEDGMENTS

D.M. was supported by the master's scholarship program at the University of Antioquia. J.F.S. was supported by the Colombian Ministry of Science, Technology and Innovation (MINCIENCIAS) through program “Sostenibilidad de sistemas ecológicos y sociales en la cuenca Magdalena-Cauca bajo escenarios de cambio climático y pérdida de bosques” (code 1115-852-70719) with receiving funds from “Patrimonio Autónomo Fondo Nacional de Financiamiento para la Ciencia, la Tecnología y la Innovación, Fondo Francisco José de Caldas”. The authors are grateful to José Posada Marín (Universidad de Antioquia) for producing Figure S1.

REFERENCES

Angarita, H., Wickel, A. J., Sieber, J., Chavarro, J., Maldonado-Ocampo, J. A., Delgado, J., & Purkey, D. (2018). Basin-scale impacts of hydropower development on the Mompós Depression wetlands, Colombia. Hydrology and Earth System Sciences, 22(5), 2839-2865.

Ayalew, T. B., Krajewski, W. F., & Mantilla, R. (2014). Connecting the power-law scaling structure of peak-discharges to spatially variable rainfall and catchment physical properties. Advances in Water Resources, 71, 32-43.

Ayalew, T. B., Krajewski, W. F., & Mantilla, R. (2015). Analyzing the effects of excess rainfall properties on the scaling structure of peak discharges: Insights from a mesoscale river basin. Water Resources Research, 51(6), 3900-3921.

Ayalew, T. B., Krajewski, W. F., Mantilla, R., & Zimmerman, D. L. (2018). Can floods in large river basins be predicted from floods observed in small subbasins?. Journal of Flood Risk Management, 11(3), 331-338.

Badia, A., Pallares-Barbera, M., Valldeperas, N., & Gisbert, M. (2019). Wildfires in the wildland-urban interface in Catalonia: Vulnerability analysis based on land use and land cover change. Science of the total environment, 673, 184-196.

Barrientos, J., Tobón, D., Villada, F., Velilla, E., & López-Lezama, J. M. (2014, September). Opportunities for seasonal forward contracts in the Colombian electricity market. In 2014 IEEE PES Transmission & Distribution Conference and Exposition-Latin America (PES T&D-LA) (pp. 1-5). IEEE.

Best, J. (2019). Anthropogenic stresses on the world's big rivers. Nature Geoscience, 12(1), 7-21.

Bolaños, S., Salazar, J. F., Betancur, T., & Werner, M. (2021). GRACE reveals depletion of water storage in northwestern South America between ENSO extremes. Journal of Hydrology, 596, 125687.

Bonnesoeur, V., Locatelli, B., Guariguata, M. R., Ochoa-Tocachi, B. F., Vanacker, V., Mao, Z., ... & Mathez-Stiefel, S. L. (2019). Impacts of forests and forestation on hydrological services in the Andes: A systematic review. Forest Ecology and Management, 433, 569-584.

Brunner, M. I., Gilleland, E., Wood, A., Swain, D. L., & Clark, M. (2020). Spatial dependence of floods shaped by spatiotemporal variations in meteorological and land-surface processes. Geophysical Research Letters, 47(13), e2020GL088000.

Brunner, M. I., Slater, L., Tallaksen, L. M., & Clark, M. (2021). Challenges in modeling and predicting floods and droughts: A review. Wiley Interdisciplinary Reviews: Water, 8(3), e1520.

Cohen, J. (1960). A coefficient of agreement for nominal scales. Educational and psychological measurement, 20(1), 37-46.

Dosdogru, F., Kalin, L., Wang, R., & Yen, H. (2020). Potential impacts of land use/cover and climate changes on ecologically relevant flows. Journal of Hydrology, 584, 124654.

Eaton, B., Church, M., & Ham, D. (2002). Scaling and regionalization of flood flows in British Columbia, Canada. Hydrological Processes, 16(16), 3245-3263.

Ellison, D., Morris, C. E., Locatelli, B., Sheil, D., Cohen, J., Murdiyarso, D., ... & Sullivan, C. A. (2017). Trees, forests and water: Cool insights for a hot world. Global Environmental Change, 43, 51-61.

ESA: Land Cover CCI Product User Guide Version 2.0, available at: http://maps.elie.ucl.ac.be/CCI/viewer/download/ ESACCI-LC-Ph2-PUGv2_2.0.pdf, last access: 10 October 2021

Farmer, W. H., Over, T. M., & Vogel, R. M. (2015). Multiple regression and inverse moments improve the characterization of the spatial scaling behavior of daily streamflows in the Southeast United States. Water Resources Research, 51(3), 1775-1796.

Formetta, G., Over, T., & Stewart, E. (2021). Assessment of peak flow scaling and its effect on flood quantile estimation in the United Kingdom. Water Resources Research, 57(4), e2020WR028076.

Funk, C., Peterson, P., Landsfeld, M., Pedreros, D., Verdin, J., Shukla, S., ... & Michaelsen, J. (2015). The climate hazards infrared precipitation with stations—a new environmental record for monitoring extremes. Scientific data, 2(1), 1-21.

Furey, P. R., Troutman, B. M., Gupta, V. K., & Krajewski, W. F. (2016). Connecting event-based scaling of flood peaks to regional flood frequency relationships. Journal of Hydrologic Engineering, 21(10), 04016037.

García-Leoz, V., Villegas, J. C., Suescún, D., Flórez, C. P., Merino-Martín, L., Betancur, T., & León, J. D. (2018). Land cover effects on water balance partitioning in the Colombian Andes: improved water availability in early stages of natural vegetation recovery. Regional Environmental Change, 18(4), 1117-1129.

Gupta, V. K., Mesa, O. J., & Dawdy, D. R. (1994). Multiscaling theory of flood peaks: Regional quantile analysis. Water Resources Research, 30(12), 3405-3421.

Gupta, V. K., & Dawdy, D. R. (1995). Physical interpretations of regional variations in the scaling exponents of flood quantiles. Hydrological Processes, 9(3-4), 347-361.

Gupta, V. K., Castro, S. L., & Over, T. M. (1996). On scaling exponents of spatial peak flows from rainfall and river network geometry. Journal of hydrology, 187(1-2), 81-104.

Gupta, V., & Waymire, E. (1998). Spatial Variability and Scale Invariance in Hydrologic Regionalization. In G. Sposito (Ed.), Scale Dependence and Scale Invariance in Hydrology (pp. 88-135). Cambridge: Cambridge University Press. doi:10.1017/CBO9780511551864.005

Gupta, V. K. (2004). Emergence of statistical scaling in floods on channel networks from complex runoff dynamics. Chaos, Solitons & Fractals, 19(2), 357-365.

Gupta, V. K., Troutman, B. M., & Dawdy, D. R. (2007). Towards a nonlinear geophysical theory of floods in river networks: an overview of 20 years of progress. Nonlinear dynamics in geosciences, 121-151.

Gupta, V. K., Mantilla, R., Troutman, B. M., Dawdy, D., & Krajewski, W. F. (2010). Generalizing a nonlinear geophysical flood theory to medium-sized river networks. Geophysical Research Letters, 37(11).

Gupta, V. K., Ayalew, T. B., Mantilla, R., & Krajewski, W. F. (2015). Classical and generalized Horton laws for peak flows in rainfall-runoff events. Chaos: An Interdisciplinary Journal of Nonlinear Science, 25(7), 075408.

Hoyos, N., Correa-Metrio, A., Sisa, A., Ramos-Fabiel, M. A., Espinosa, J. M., Restrepo, J. C., & Escobar, J. (2017). The environmental envelope of fires in the Colombian Caribbean. Applied Geography, 84, 42-54.

Hoyos, N., Escobar, J., Restrepo, J. C., Arango, A. M., & Ortiz, J. C. (2013). Impact of the 2010–2011 La Niña phenomenon in Colombia, South America: the human toll of an extreme weather event. Applied Geography, 39, 16-25.

Ishak, E., Haddad, K., Zaman, M., & Rahman, A. (2011). Scaling property of regional floods in New South Wales Australia. Natural Hazards, 58(3), 1155-1167.

Jarvis, A., Reuter, H. I., Nelson, A., & Guevara, E. (2008). Hole-filled SRTM for the globe Version 4. available from the CGIAR-CSI SRTM 90m Database (http://srtm. csi. cgiar. org), 15, 25-54.

Latrubesse, E. M., Arima, E. Y., Dunne, T., Park, E., Baker, V. R., d'Horta, F. M., ... & Stevaux, J. C. (2017). Damming the rivers of the Amazon basin. Nature, 546(7658), 363-369.

Li, D., Long, D., Zhao, J., Lu, H., & Hong, Y. (2017). Observed changes in flow regimes in the Mekong River basin. Journal of Hydrology, 551, 217-232.

Li, W., Ciais, P., MacBean, N., Peng, S., Defourny, P., & Bontemps, S. (2016). Major forest changes and land cover transitions based on plant functional types derived from the ESA CCI Land Cover product. International journal of applied earth observation and geoinformation, 47, 30-39.

Lima, C. H., AghaKouchak, A., & Lall, U. (2017). Classification of mechanisms, climatic context, areal scaling, and synchronization of floods: The hydroclimatology of floods in the upper Paraná River basin, Brazil. Earth System Dynamics, 8(4), 1071-1091.

Mandapaka, P. V., Krajewski, W. F., Mantilla, R., & Gupta, V. K. (2009). Dissecting the effect of rainfall variability on the statistical structure of peak flows. Advances in Water Resources, 32(10), 1508-1525.

Mantilla, R., Gupta, V. K., & Mesa, O. J. (2006). Role of coupled flow dynamics and real network structures on Hortonian scaling of peak flows. Journal of Hydrology, 322(1-4), 155-167.

Mekonnen, D. F., Duan, Z., Rientjes, T., & Disse, M. (2018). Analysis of combined and isolated effects of land-use and land-cover changes and climate change on the upper Blue Nile River basin's streamflow. Hydrology and earth system sciences, 22(12), 6187-6207.

Menabde, M., Veitzer, S., Gupta, V., & Sivapalan, M. (2001). Tests of peak flow scaling in simulated self-similar river networks. Advances in Water Resources, 24(9-10), 991-999.

Modarres, R. (2010). Low flow scaling with respect to drainage area and precipitation in Northern Iran. Journal of Hydrologic Engineering, 15(3), 210-214.

Montanari, A., Young, G., Savenije, H. H. G., Hughes, D., Wagener, T., Ren, L. L., ... & Belyaev, V. (2013). "Panta Rhei—everything flows": change in hydrology and society—the IAHS scientific decade 2013–2022. Hydrological Sciences Journal, 58(6), 1256-1275.

Nowosad, J., Stepinski, T. F., & Netzel, P. (2019). Global assessment and mapping of changes in mesoscale landscapes: 1992–2015. International Journal of Applied Earth Observation and Geoinformation, 78, 332-340.

Ogden, F. L., & Dawdy, D. R. (2003). Peak discharge scaling in small Hortonian watershed. Journal of Hydrologic Engineering, 8(2), 64-73.

Peña-Arancibia, J. L., Bruijnzeel, L. A., Mulligan, M., & Van Dijk, A. I. (2019). Forests as 'sponges' and 'pumps': Assessing the impact of deforestation on dry-season flows across the tropics. Journal of Hydrology, 574, 946-963.

Perez, G., Mantilla, R., Krajewski, W. F., & Wright, D. B. (2019). Using physically based synthetic peak flows to assess local and regional flood frequency analysis methods. Water Resources Research, 55(11), 8384-8403.

Perez, G., Mantilla, R., & Krajewski, W. F. (2018). The influence of spatial variability of width functions on regional peak flow regressions. Water Resources Research, 54(10), 7651-7669.

Perez, G., Mantilla, R., & Krajewski, W. F. (2018). Spatial patterns of peak flow quantiles based on power-law scaling in the Mississippi River basin. In Advances in nonlinear geosciences (pp. 497-518). Springer, Cham.

Perez, G., Mantilla, R., Krajewski, W. F., & Quintero, F. (2019). Examining observed rainfall, soil moisture, and river network variabilities on peak flow scaling of rainfall-runoff events with implications on regionalization of peak flow quantiles. Water Resources Research, 55(12), 10707-10726.

Poveda, G., Vélez, J., Mesa, O., Hoyos, C., Mejía, F., Barco, O., & Correa, P. (2002). Influencia de fenómenos macroclimáticos sobre el ciclo anual de la hidrología colombiana: cuantificación lineal, no lineal y percentiles probabilísticos. Meteorología Colombiana, 6, 121-130.

Restrepo, J. D., Kettner, A. J., & Syvitski, J. P. (2015). Recent deforestation causes rapid increase in river sediment load in the Colombian Andes. Anthropocene, 10, 13-28.

Restrepo, J. D., & Kjerfve, B. (2000). Magdalena river: interannual variability (1975–1995) and revised water discharge and sediment load estimates. Journal of hydrology, 235(1-2), 137-149.

Rodríguez, E., Salazar, J. F., Villegas, J. C., & Mercado-Bettín, D. (2018). Assessing changes in extreme river flow regulation from non-stationarity in hydrological scaling laws. Journal of Hydrology, 562, 492-501.

Salazar, J. F., Villegas, J. C., Rendón, A. M., Rodríguez, E., Hoyos, I., Mercado-Bettín, D., & Poveda, G. (2018). Scaling properties reveal regulation of river flows in the Amazon through a “forest reservoir”. Hydrology and Earth System Sciences, 22(3), 1735-1748.

Save, H., Bettadpur, S., & Tapley, B. D. (2016). High-resolution CSR GRACE RL05 mascons. Journal of Geophysical Research: Solid Earth, 121(10), 7547-7569.

Tananaev, N. I., Makarieva, O. M., & Lebedeva, L. S. (2016). Trends in annual and extreme flows in the Lena River basin, Northern Eurasia. Geophysical Research Letters, 43(20), 10-764.

Urrea, V., Ochoa, A., & Mesa, O. (2019). Seasonality of rainfall in Colombia. Water Resources Research, 55(5), 4149-4162.

Vogel, R. M., & Sankarasubramanian, A. (2000). Spatial scaling properties of annual streamflow in the United States. Hydrological sciences journal, 45(3), 465-476.

Watkins, M. M., Wiese, D. N., Yuan, D. N., Boening, C., & Landerer, F. W. (2015). Improved methods for observing Earth's time variable mass distribution with GRACE using spherical cap mascons. Journal of Geophysical Research: Solid Earth, 120(4), 2648-2671.

Weng, W., Becker, S. L., Lüdeke, M. K., & Lakes, T. (2020). Landscape matters: Insights from the impact of mega-droughts on Colombia's energy transition. Environmental Innovation and Societal Transitions, 36, 1-16.

Yue, S., & Wang, C. Y. (2004). Scaling of Canadian low flows. Stochastic Environmental Research and Risk Assessment, 18(5), 291-305.

Zhang, L., Cheng, L., Chiew, F., & Fu, B. (2018). Understanding the impacts of climate and land use change on water yield. Current Opinion in Environmental Sustainability, 33, 167-174.

Supplementary material for

"Scaling theory reveals weak and changing river flow regulation in a medium-size tropical basin"

Diver E. Marín [1*] and Juan F. Salazar [1]

[1] GIGA, Escuela Ambiental, Facultad de Ingeniería, Universidad de Antioquia, Medellín-Colombia

Corresponding Author: diver.marin@udea.edu.co

Contents of this file:

Supplementary information S1

Figures S1 to S4

Tables S1 to S3

Supplementary information 1

$$\boldsymbol{P_C} = \sum \frac{\boldsymbol{C_{ii}}}{\boldsymbol{n}} \quad (1)$$

$$\boldsymbol{P_a} = \sum \frac{\boldsymbol{C_{.i} * C_{i.}}}{\boldsymbol{n^2}} \quad (2)$$

$$\boldsymbol{K} = \sum \frac{\boldsymbol{P_C - P_a}}{\boldsymbol{1 - P_a}} \quad (3)$$

To calculate the Kappa Index, a square matrix is built, its size is given by the number of categories of land use/cover (N). The values of the main diagonal (C_{ii}) represent the pixels in which there was no change in the particular category of land use/cover (i). The values on the outside of the main diagonal (C_{ij}) represent the pixels in which the land use/cover becomes of the category i in the map 1 to the category j in the map 2. Marginal values are calculated as the sum of each row or col, and they will be equal to the total area classified in each category by map. To calculate the Kappa index (K) it is necessary to estimate the proportion (P_c) and the proportion expected by randomness (P_a) (Equation 1 and Equation 2 respectively), next using the Equation 3 the concordance value is calculated. The Kappa matrix allows us to characterize

rates, probabilities of occurrence, patterns and behaviors in the land use/cover change (Badia et al., 2019; Cohen, 1960; Table S1).

Table S1. Concordance´s matrix of Kappa.

	Map 1				
Map 2	**1**	**2**	**...**	**N**	**Marginal**
1	C 11	C 12	...	C 1N	C 1.
2	C 21	C22	...	C 2N	C 2.
.	.			.	.
.	.			.	.
.	.			.	.
N	C N1	C N2	...	C NN	C N.
Marginal	C .1	C .2	...	C. N	n

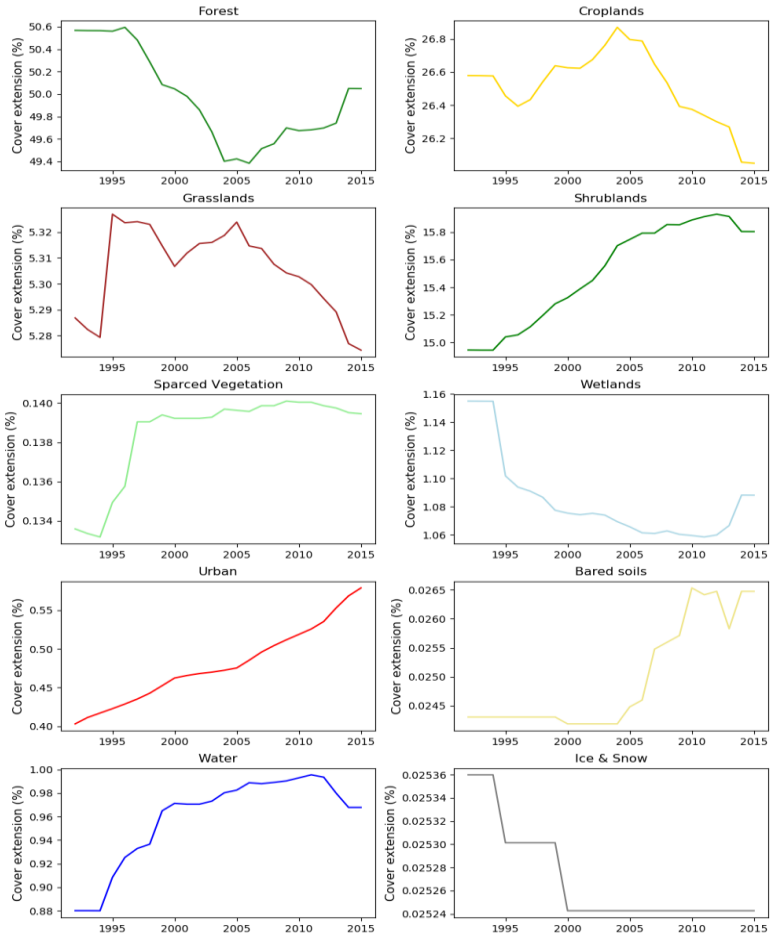

Supplementary figure S1. Times series of cover types in the MRB basin for the period 1992-2015.

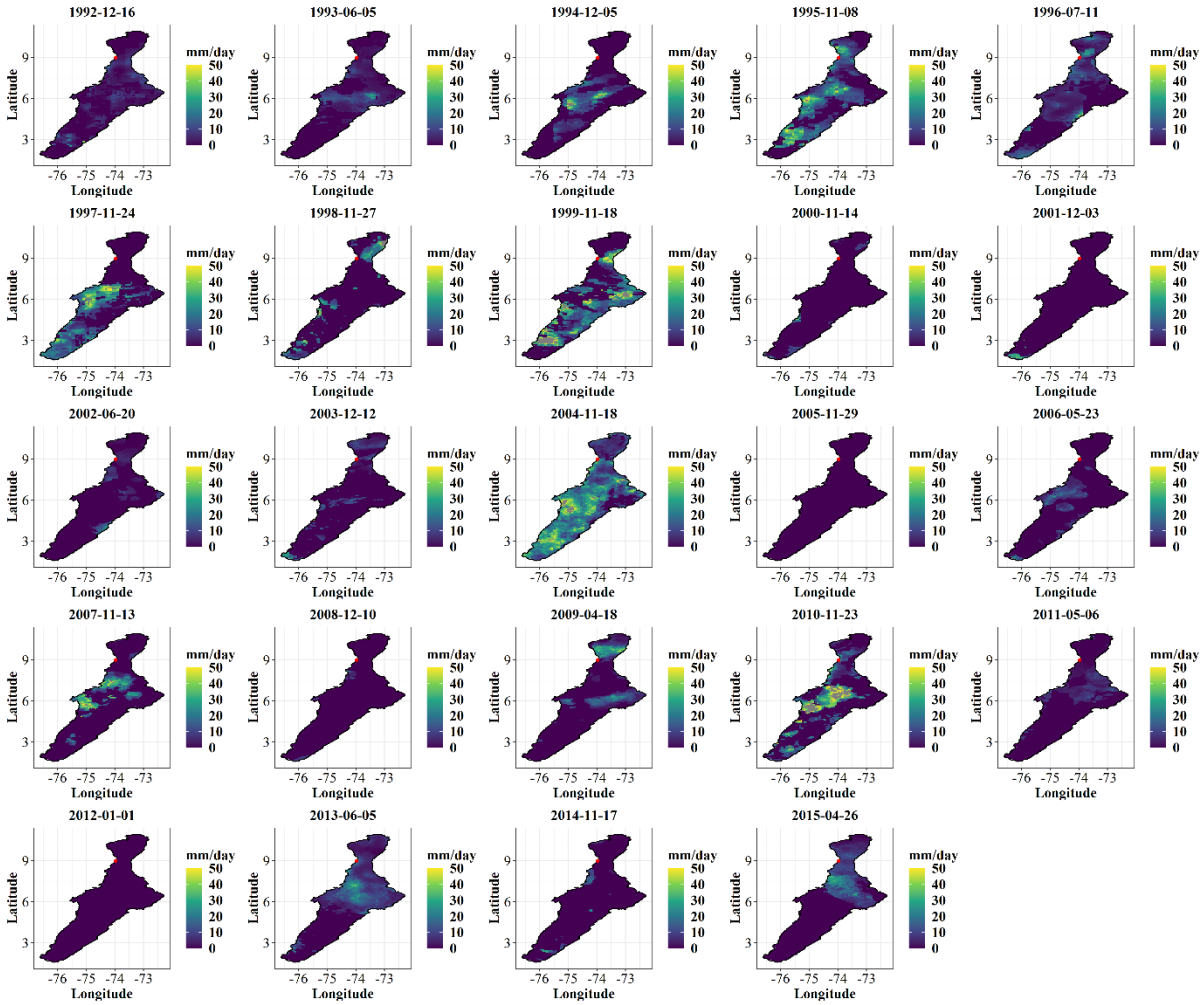

Supplementary figure S2. Daily precipitation for each event during 1992-2015. The red point represents the basin´s outlet.

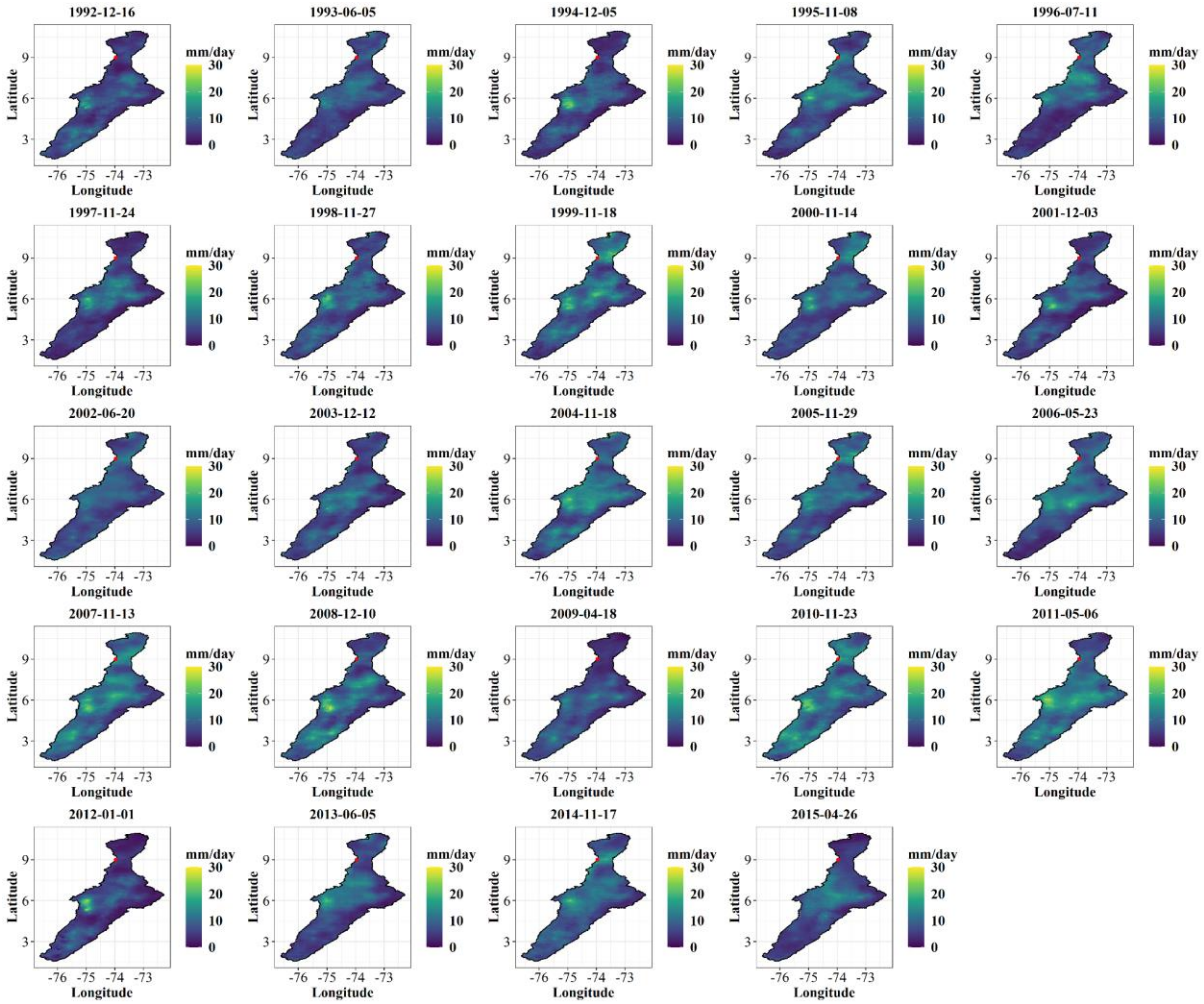

Supplementary figure S3. 30-day accumulated precipitation by event in mm/day. The red point represents the basin´s outlet.

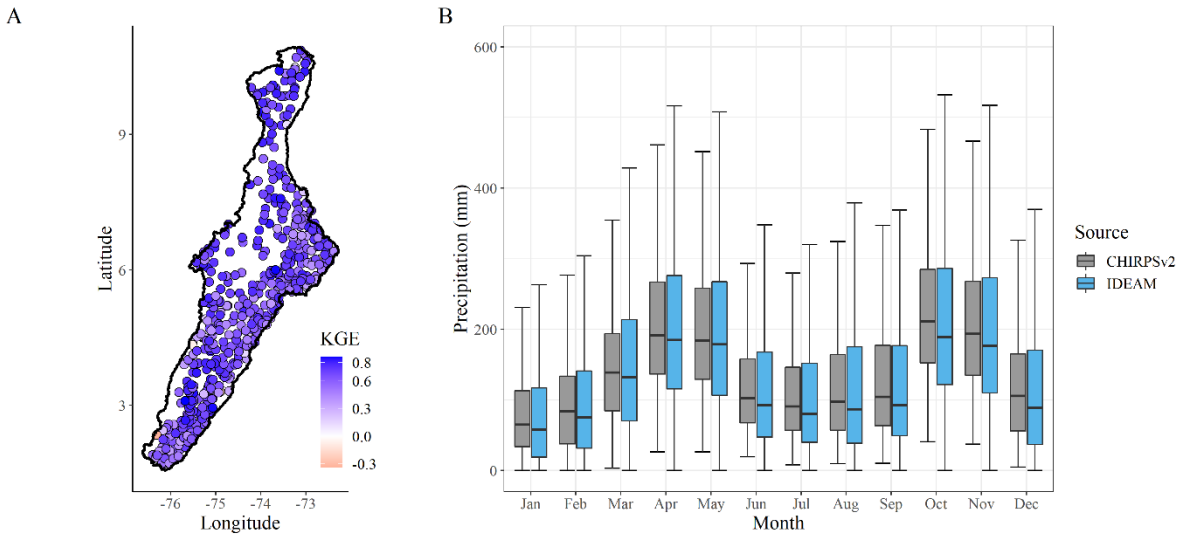

Supplementary figure S4. A) Modified Kling-Gupta efficiency (KGE') at monthly scale using CHIRPSv2 and B) mean annual precipitation cycle comparison using CHIRPSv2 and IDEAM data for MRB.

Table S2. Summary of scaling statistics for high (β_F) and low (β_L) flows

Year	β_L	ln(α)	R^2	p value	β_F	ln(α)	R^2	p value
1992	1.07	-5.16	0.85	2.92E-09	1.08	-4.66	0.85	2.06E-09
1993	1.10	-5.29	0.83	7.76E-09	1.10	-4.61	0.9	3.11E-11
1994	1.11	-4.96	0.86	1.70E-09	1.07	-4.22	0.88	3.15E-10
1995	1.04	-4.85	0.85	6.24E-09	1.04	-3.83	0.83	6.81E-09
1996	1.13	-5.17	0.83	1.33E-08	1.06	-3.85	0.9	9.23E-11
1997	0.97	-4.45	0.81	6.13E-08	1.02	-4.20	0.83	6.35E-09
1998	1.03	-4.97	0.81	1.05E-07	1.07	-4.08	0.86	7.79E-10
1999	1.04	-3.86	0.85	3.16E-09	0.94	-2.67	0.83	1.49E-08
2000	1.15	-5.22	0.88	1.68E-10	1.01	-3.79	0.86	1.65E-09
2001	1.10	-5.27	0.83	1.11E-08	1.14	-4.51	0.86	1.76E-09
2002	1.10	-5.12	0.85	7.38E-09	1.07	-3.96	0.85	3.33E-09
2003	1.02	-4.61	0.81	8.90E-08	1.05	-4.04	0.9	1.37E-10
2004	1.05	-4.59	0.81	3.30E-08	0.99	-2.72	0.85	1.07E-08
2005	1.18	-5.55	0.81	1.96E-08	0.98	-3.34	0.85	2.07E-09
2006	1.10	-4.99	0.83	8.15E-09	1.00	-3.51	0.88	1.92E-10
2007	0.96	-4.06	0.79	4.14E-07	1.05	-3.45	0.86	6.19E-10
2008	1.12	-5.19	0.79	5.41E-08	1.11	-4.35	0.92	9.96E-12

2009	1.04	-4.38	0.83	8.73E-09	1.10	-4.42	0.85	8.38E-09
2010	0.98	-4.40	0.74	6.76E-07	1.06	-3.44	0.94	5.89E-13
2011	1.01	-3.85	0.86	1.07E-09	1.07	-3.58	0.96	3.88E-14
2012	0.99	-4.06	0.9	1.80E-10	1.09	-4.22	0.88	4.58E-10
2013	1.03	-4.53	0.81	1.98E-08	1.10	-4.63	0.83	1.04E-08
2014	1.05	-4.42	0.83	1.27E-08	1.02	-3.79	0.9	6.37E-11
2015	1.01	-5.02	0.81	3.75E-08	1.12	-4.75	0.81	2.49E-08

Table S3. Summary of moving averages scaling statistics for low (β_L) and high (β_F) flows.

Moving average	**Evento**	**β_L**	**p value**	**R^2**	**β_F**	**p value**	**R^2**
n=2	1	1.07	3.7E-09	0.85	1.09	1.2E-10	0.89
	2	1.09	2.0E-09	0.86	1.08	8.8E-11	0.90
	3	1.07	1.7E-09	0.86	1.05	1.0E-09	0.87
	4	1.09	7.9E-09	0.83	1.04	2.8E-10	0.88
	5	1.06	4.0E-08	0.82	1.04	1.2E-10	0.89
	6	1.00	3.4E-07	0.81	1.05	1.1E-09	0.86
	7	1.05	7.1E-09	0.87	0.98	4.0E-09	0.84
	8	1.08	4.1E-10	0.88	0.95	9.9E-09	0.85
	9	1.12	6.3E-10	0.87	1.06	6.9E-10	0.89

	10	1.10	2.9E-09	0.87	1.09	1.1E-09	0.86
	11	1.05	1.5E-08	0.84	1.04	3.7E-10	0.89
	12	1.02	1.9E-08	0.83	1.01	1.1E-09	0.89
	13	1.11	1.6E-08	0.82	0.97	8.7E-10	0.88
	14	1.14	1.1E-08	0.83	0.98	2.6E-10	0.88
	15	1.03	1.5E-07	0.81	1.02	1.1E-10	0.89
	16	1.02	2.0E-07	0.80	1.05	1.5E-11	0.91
	17	1.06	8.6E-09	0.83	1.10	2.6E-10	0.90
	18	1.01	3.8E-08	0.80	1.05	6.5E-12	0.93
	19	1.00	7.4E-09	0.83	1.06	1.4E-14	0.96
	20	1.00	3.0E-11	0.92	1.06	1.3E-13	0.95
	21	0.99	5.7E-10	0.89	1.08	3.6E-10	0.88
	22	1.03	6.0E-09	0.84	1.05	2.6E-10	0.88
	23	1.04	7.4E-09	0.83	1.05	4.7E-10	0.88
n=3	1	1.08	1.9E-09	0.86	1.08	1.6E-10	0.89
	2	1.07	1.9E-09	0.86	1.06	2.8E-10	0.88
	3	1.09	2.8E-09	0.85	1.05	2.2E-10	0.89
	4	1.06	3.5E-08	0.82	1.03	3.8E-10	0.88
	5	1.06	2.1E-07	0.82	1.05	1.6E-10	0.89

	6	1.04	3.8E-08	0.86	0.98	3.5E-09	0.85
	7	1.09	2.4E-09	0.88	0.98	4.3E-09	0.86
	8	1.08	4.8E-10	0.88	1.01	4.0E-09	0.86
	9	1.12	3.7E-10	0.89	1.05	9.8E-10	0.88
	10	1.06	6.5E-09	0.85	1.05	3.1E-10	0.89
	11	1.04	1.1E-08	0.84	1.01	1.9E-09	0.89
	12	1.08	1.0E-08	0.84	1.01	6.6E-10	0.90
	13	1.11	1.1E-08	0.83	0.97	3.4E-10	0.89
	14	1.07	1.3E-07	0.81	1.01	1.8E-10	0.89
	15	1.04	1.3E-07	0.81	1.04	1.6E-11	0.91
	16	1.01	8.8E-08	0.82	1.05	1.1E-10	0.91
	17	1.03	2.5E-08	0.81	1.07	5.0E-12	0.93
	18	1.01	6.3E-09	0.84	1.06	2.3E-13	0.95
	19	0.99	2.7E-10	0.90	1.06	6.2E-14	0.95
	20	1.00	1.0E-10	0.91	1.06	3.5E-13	0.94
	21	1.02	2.5E-10	0.90	1.06	1.3E-10	0.89
	22	1.02	5.6E-09	0.84	1.06	7.4E-10	0.87
n=4	1	1.07	1.7E-09	0.86	1.06	3.4E-10	0.88
	2	1.09	2.7E-09	0.85	1.06	1.0E-10	0.89

	3	1.07	1.7E-08	0.84	1.04	2.9E-10	0.88
	4	1.06	2.0E-07	0.82	1.04	3.6E-10	0.88
	5	1.07	3.9E-08	0.86	0.99	5.2E-10	0.87
	6	1.08	1.8E-08	0.87	0.99	4.9E-09	0.86
	7	1.09	3.2E-09	0.88	1.02	2.5E-09	0.87
	8	1.09	4.8E-10	0.89	1.01	3.0E-09	0.86
	9	1.09	1.2E-09	0.88	1.05	1.2E-09	0.89
	10	1.05	5.2E-09	0.86	1.03	2.2E-09	0.88
	11	1.08	8.1E-09	0.85	1.01	1.0E-09	0.89
	12	1.08	6.6E-09	0.85	1.00	5.6E-10	0.90
	13	1.05	1.1E-07	0.82	0.99	4.1E-10	0.89
	14	1.07	1.3E-07	0.81	1.02	4.0E-11	0.90
	15	1.03	7.8E-08	0.82	1.04	9.9E-11	0.91
	16	1.00	2.0E-07	0.80	1.05	1.2E-11	0.93
	17	1.03	6.9E-09	0.84	1.07	4.1E-13	0.95
	18	1.00	3.2E-10	0.89	1.06	8.0E-13	0.95
	19	1.00	4.5E-10	0.89	1.05	7.4E-14	0.95
	20	1.01	6.3E-11	0.91	1.05	4.3E-13	0.94
	21	1.01	2.7E-10	0.90	1.07	2.9E-10	0.88

n=5	1	1.08	2.2E-09	0.85	1.06	1.4E-10	0.89
	2	1.07	1.7E-08	0.84	1.05	1.5E-10	0.89
	3	1.07	1.0E-07	0.84	1.05	3.0E-10	0.88
	4	1.06	4.4E-08	0.85	1.00	7.2E-10	0.87
	5	1.09	2.3E-08	0.86	1.00	1.4E-09	0.88
	6	1.09	2.3E-08	0.86	1.02	3.0E-09	0.86
	7	1.09	3.6E-09	0.89	1.02	2.2E-09	0.87
	8	1.07	8.5E-10	0.88	1.01	3.9E-09	0.88
	9	1.07	1.5E-09	0.88	1.03	1.6E-09	0.89
	10	1.08	4.8E-09	0.86	1.03	1.3E-09	0.89
	11	1.08	5.7E-09	0.85	1.00	6.8E-10	0.90
	12	1.04	3.5E-08	0.86	1.02	6.7E-10	0.90
	13	1.05	1.1E-07	0.82	1.01	1.2E-10	0.91
	14	1.05	8.3E-08	0.82	1.03	1.9E-10	0.90
	15	1.01	1.5E-07	0.81	1.04	1.8E-11	0.92
	16	0.99	7.4E-08	0.83	1.05	6.6E-13	0.95
	17	1.02	5.6E-10	0.89	1.07	1.1E-12	0.94
	18	1.00	4.7E-10	0.89	1.06	1.1E-12	0.94
	19	1.01	2.2E-10	0.90	1.05	1.0E-13	0.95

	20	1.01	7.5E-11	0.91	1.05	1.4E-12	0.93

References

Badia, A., Pallares-Barbera, M., Valldeperas, N., & Gisbert, M. (2019). Wildfires in the wildland-urban interface in Catalonia: Vulnerability analysis based on land use and land cover change. Science of the total environment, 673, 184-196.

Cohen, J. (1960). A coefficient of agreement for nominal scales. Educational and psychological measurement, 20(1), 37-46.